

Peer review status:

This is a non-peer-reviewed preprint submitted to EarthArXiv.

Sanjay Karthick Avva (Submitter, Co-Author): https://orcid.org/0009-0000-4901-5738 Muhammad Moosa Awais (Co-Author): https://orcid.org/0009-0008-7901-4355

A COMPUTER VISION FRAMEWORK FOR ESTIMATING SURFACE HABITABILITY FROM MARS USING CONVOLUTIONAL ANALYSIS

Muhammad Moosa Awais^{1†}, Sanjay Avva^{2†}*

- 1. Morris County School of Technology, 400 E Main St, Denville, NJ, 07834, United States
- 2. Morris County School of Technology, 400 E Main St, Denville, NJ, 07834, United States
- [†] These authors contributed equally to this work.
- * Corresponding author email: muhammad.moosa.awais@gmail.com

ABSTRACT

Identifying signs of life in extraterrestrial environments is one of the growing challenges in planetary science. Conventional approaches of detecting habitability rely heavily on direct contact with biosignatures or geological analyses, but limited data and mission costs hold back such methods. This work introduces a computer vision-based pipeline that analyzes planetary surface images to determine a livability index that estimates the photographed terrain's likelihood to support life. The data is from the Mars Surface Image Dataset (collected by NASA's Curiosity Rover) and the Mars Handlens Analog Database (archived at the PDS Geosciences Node of Washington University in St. Louis). Unlike existing binary classifiers that only distinguish between planetary sources, our method utilizes feature extraction to evaluate environments in terms of their habitability. By combining convolutional features with descriptors of texture, hue, and structure, we demonstrate that our model can move beyond simple classification and instead generate interpretable, probabilistic estimates of habitability. With a livability index, we can focus on key habitability features and use them to guide targeted exploration to better search for life beyond Earth.

KEYWORDS

Computer-Vision; Astrobiology; Mars; Habitability Analysis; Convolutional Neural Network; Geomorphic Feature Extraction; Scikit-image

INTRODUCTION

Missions to planets like Mars have created large datasets of high quality planetary imagery. From aquatic regions to sedimentary outcrops, these images cover expansive planetary terrain. These images contain essential visual environmental data that can be used to push efforts in astrobiology, yet most computational pipelines do not fully utilize them beyond archives for manual analysis or determinants for planetary origin. Such methodologies, though useful, do not provide the detailed environmental insight needed to evaluate the biological potential of such an environment.

To address this, we developed a pipeline powered by a convolutional neural network (CNN) to extract and classify environmental features in planetary images. The model focuses on finding relevant terrain patterns, such as clasts and stratification, in order to determine proxies that evidence life. These features are highly synonymous with the presence of life and potentially habitable conditions (13).

By leveraging deep learning, the pipeline can move beyond a simple binary classification of planetary surfaces and instead provide a probabilistic assessment of habitability through the reported livability index.

This framework posits a new opportunity for how visual technologies may advance planetary studies in the field of biological science. Current geological practices of manually annotating images or designing task-specific classifiers that address shallow questions lack scalability and can overlook subtle environmental indicators that are integral during classification. This approach offers a more scalable and data-driven alternative to time-consuming geological annotation. It can also reduce the extensive labor needed to detect complex visual signals imperceptible to human observation. To that end, the credibility of contemporary habitability assessments can be improved.

Additionally, planetary missions continue to create larger and more sophisticated datasets (such as those from NASA's Mars Handlens and Curiosity Rover libraries). As such, the need for more robust, automated analytical tools and approaches is distinctly increasing. Manual curation is infeasible at such a scale, and a lack of productive pipelines may underutilize the depth of the available data. An approach that incorporates advanced ML methodologies could rectify this problem by accelerating data evaluation. It could also help engineers make better decisions about sampling priorities, landing site selections, and other long-term strategies.

In doing so, the framework offers a general technique that can be applied to other fields where visual analysis is necessary. Beyond its intuitiveness, this pipeline demonstrates how machine learning and computer vision can be used as powerful tools to address the fundamental question of astrobiology: could life not only exist, but thrive, in an extraterrestrial setting?

MATERIALS AND METHODOLOGY

This study investigates whether computer vision techniques can be utilized to analyze and evaluate geomorphic proxies of surface habitability on Mars. The goal was not only to systematically calculate images as representative of Mars or Analog (Earthly ecosystems that posit life but additionally share celestial attributes) environments, but also to extract quantitative features that use computer vision algorithms to substantiate potential evidence of conditions relevant to habitability, whilst testing the usage potential for feature analysis in the future. To achieve this, the project relied on external qualitative secondary data from NASA's open data portal and PDS libraries. Because the research objective aimed to detect and examine measurable visual proxies, image data proved an appropriate medium to establish a pilot study. The methodological approach combined an experimental stage, in which a CNN was trained and validated to linearly distinguish Earth from Mars images, followed by a synopsis stage where computed features were transformed into proxy scores and aggregated into a livability index based on a tuned pilot-based weights system that was tested and inferred based on geomorphic plausibility of livable conditions (visually interpretable factors that make earth livabile).

Input data from this study were drawn from two publicly available archives, both provided by NASA. The first was the Mars Surface Image Dataset [Curiosity Rover, Labeled Data Set Ver 1] (1), which contains 6,691 labeled Mars images across 24 surface channels, collected by NASA's Jet Propulsion Laboratory and available at their data portal. For the purposes of this study, a randomly selected subset of 1,302 images was chosen for analysis, in order to preserve image diversity while keeping in mind the computational limits at hand. The second collection of data, the Mars Handlens Analog Image Database (2), includes a collection of high-resolution terrestrial samples archived at the PDS Geosciences Node of Washington University in St. Louis. Both sources were available through public domain and were selected for analysis for this project because they provide complementary perspectives that could highlight intricate patterns through visual technologies.

After data collection, photographs of the Mars surface snapshots and the analog Earth snapshots were organized into separate image arrays and directories after being filtered to only process common formats (PNG, JPEG, JPG). Afterwards, each array is marked with its own binary label and then subsequently returned as a singular tuple, which would later be used for classifier training.

Within the experimental stage (Stage I), all images are preprocessed with OpenCV (3) and scikit-image (4) to maintain consistency. Each image was resized to a 128x128px, and pixel intensities were additionally normalized to a range of [0,1] as a method of standardizing data for CNN training. High-resolution analog samples were mapped into representative regions to preserve texture without introducing scale bias. The primary flow of the first stage in the study involved training a CNN implemented in TensorFlow/Keras (5) to distinguish Martian imagery from Earth analogs. The CNN consisted of three convolutional layers (16-32-64), utilizing the ReLU activation function in order to analyze complex textures and edges. The model then combined global average pooling, a dense layer of roughly 64 units, and a final softmax classification, outputting two endpoint classes and a similarity score that determined whether the image classified was "Mars-like" or "Earth-Analog".

The model was trained using the Adam optimizer (17) with cross-entropy loss. We used an 80/20 train-validation split over 100 epochs with scaled termination to avoid overfitting. For inference, the model outputs a probability distribution such that p=[p0,p1], where the greater predicted label was finalized by \hat{y} =argmaxipi, along with its associated confidence rate. Model outputs were then further supported by the centroid of Mars features using calculated cosine similarity:

$$sim(F, \mu_{mars}) = \frac{F \cdot \mu_{mars}}{\|F\| \|\mu_{mars}\|}$$

This value ranges between 0 and 1, with values nearer to 1 indicating the image feature's strong connection to the average Mars representation.

Within the synopsis stage of the pipeline (Stage II), the focus of the model shifts from categorical classification to a proxy-based livability analysis that provides addressable features. As previously mentioned, images that were flagged as Mars-like underwent more intensive feature extraction used to quantify seven distinct geomorphic and photometric indicators. These included the presence/detection of:

- Stratification[Rock or Wind deposits arranged in distinct layers]
- Channel Ridges [Raised ridges resembling dried riverbeds/channels]

- Periodic Ripples [Repeating wave patterns in sand and sediment]
- Dust Cover [Layers of fine particles covering the surface, disseminates biosignatures]
- Clasts breakages [Distribution of rock fragments in soil or deposits]
- Hanging Alcoves [Sheltered depressions or overhangs]
- Fluvial Texture-Complexity [Patterns expressing presence of liquid]

These indicators were specifically chosen, as they are universally agreed to heavily correlate with the presence of life (13).

Each indicator produced a raw metric m_k , which was mapped into a bounded proxy score $s_k \in [0, 1]$ using either sigmoid functions or Gaussian preference curves based on the proxy's expected relationship with surface livability.

The classifier estimated stratified layering by counting the frequency of repeated near-parallel line segments found using the Hough transform (5) and computing the variance level of their angles:

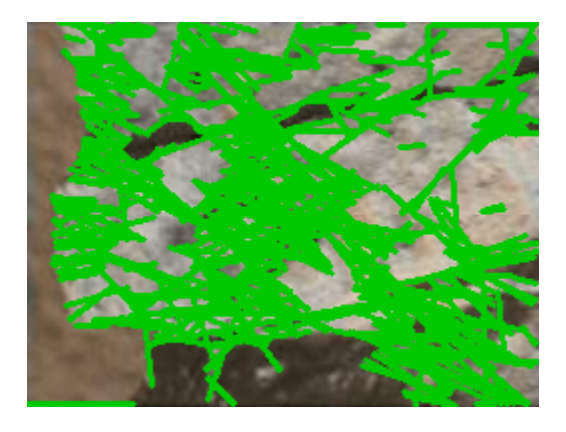


(Figure 1) Hough Line Segments

The resulting score increased with greater line density and decreased with higher angular deviation, where $\sigma(x; \text{mid}, \text{steep}) = 1/(1 + e^{-steep(x-mid)})$ is the logistic sigmoid of o^{-1} is its inverse form.

This method highlights images that contain the presence of consistent parallel stratification while, in turn, penalizing inputs with highly variable line orientations not signifiable to stable erosion where deposition is not present.

Channel-like ridges were found using the Frangi ridge filter (7) followed by applying skeletonization (8). Three raw metrics in total were then observed: total ridge length (m_{ridge}) , number of branching points (m_{branch}) , and a sinuosity proxy based on gradient magnitude around the medial axis. Higher values of these indicators proved potentially branched, extended, or curved ridge systems, consistent with channel features formed by external fluvial movement (15).

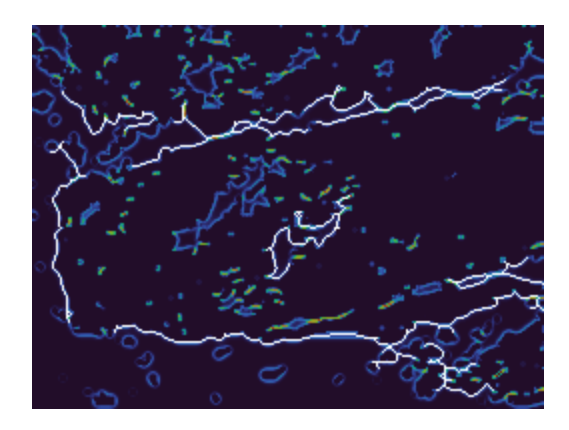


(Figure 2) Skeletonized ridge networks drawn over Frangi mapping

In order to identify the presence of periodic ripples, a bank of Gabor filters (9) is applied across numerous orientations ($\theta \in \{0^\circ, 30^\circ, 60^\circ, 90, 120^\circ, 150^\circ\}$) along with a set of wavelengths ($\lambda \in \{8,12,16,24,32,48\}$). The mean filter responses were then used to choose the most dominant wavelength λ^* , while the orientation dispersion *od* was utilized to quantify alignment. To return a proxy score, the dominant wavelength is then compared to an empirically chosen aeolian ripple scale of about 18px using a Gaussian preference curve, while the aforementioned dispersion of *od* penalizes misaligned patterns in score calculation:

$$s_{ripples} = \exp\left(-\frac{(\lambda * - 24)^2}{2 \cdot 12^2}\right) \cdot (1 - clip(od, 0, 1))$$

Dust cover proxies were analyzed from Shannon entropy (10) and local variance statistics, mainly through the calculation of RMS values that determine an input's flatness. Images with higher ratios of low-entropy and low-variance patches were scored as dust-covered, as such conditions typically confuse surface features and therefore signify low entropy. Evidence of this indicator was weighted as 0.0 in the composite index score; however, its proxy evaluations were still noted in the testing phase.

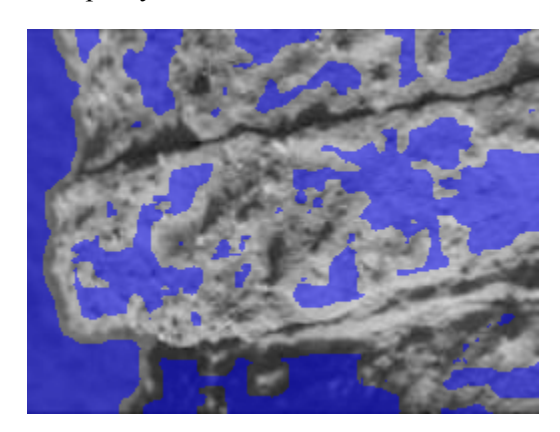


(Figure 3) Low variance mask outlining areas of uniform noisy texture

Clast distribution was estimated by detecting high-frequency residuals after applying a Gaussian blur, which highlighted edges similar to those found in rock fragments. A binary rock mask was constructed by thresholding deviations from the mean intensity, and morphological operations were used to remove noise. Contours of clasts were then extracted, and their total area was normalized by the full image area to compute piece-by-piece rock cover.

Moderate clast cover was scored highest using a Gaussian preference centered at 12% of D_{50} and D_{84} (50th and 84th percentile clast sizes) were also recorded.



(Figure 4) Detected Clast Contours

Shadowed alcoves were identified by patches of shadow intersecting with regions of depression. Shadows were defined as grayscale pixels below the mean minus 80% of the standard deviation. While concavities were mapped using the Laplacian operator (16) to capture depressions. A binary mask of concave shadowed regions was also created, and the fraction of such pixels was mapped to a proxy score using a steep sigmoid.



(Figure 5) Laplacian Alcoves Mapping

Fluvial texture complexity from the rover input images was assessed using two main factors: fractal dimension and multiscale roughness. Fractal dimension was found using a derived box-counting method on Canny Edges (11), where the slope of the log-log plot of occupied boxes vs. scale noted the dimension. Roughness was computed as the average Laplacian-of-Gaussian (LoG) (16) energy across multiple

Gaussian smoothing scales. These metrics were combined into a weighted proxy score that weighed terrain with complex branching structure and multi-scale variability as more "liveable" than others.

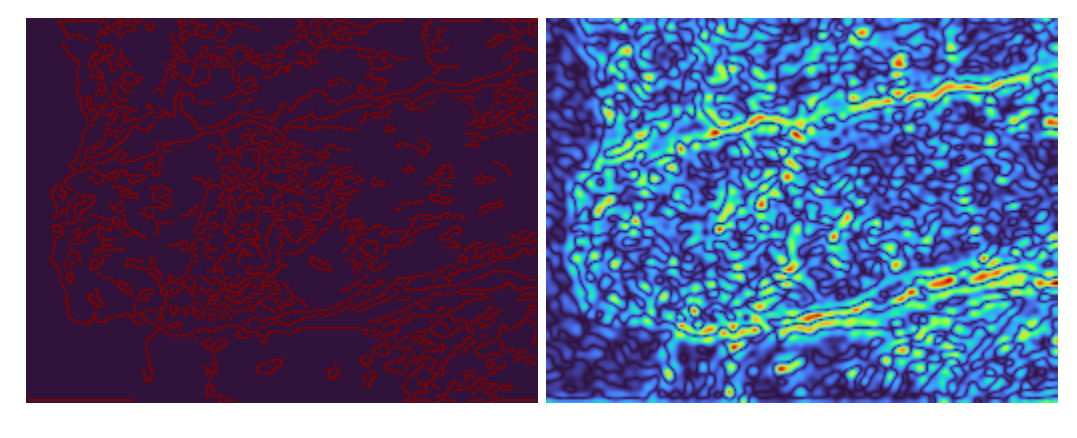


(Figure 6) Canny edge detection map

(Figure 7) LoG energy map

Then, in the final livability index, all proxy scores were aggregated into a quantitative measure of surface habitability likelihood, using a weighted linear combination bounded between 0 and 1 that weighed collected values against a set of empirically pilot-determined biases. Positive geomorphic indicators (layering channels, ripples, clasts, shelters, and fluvial complexity) affected the score, while the sole negative indicator of dust had no impact on the final result. The index serves as a reproducible classification of geomorphic and photometric proxies, acting as a pilot between raw image categorization and providing means of proxies for astrobiological inference in the future.

TESTING AND RESULTS

We trained a lightweight CNN (3 convolutional blocks, 16-32-64 filters with ReLU; global average pooling; 64-unit dense layer; softmax) to discriminate between Mars and Earth-analog /Earth environments. The model was run on an 80-20 split for 100 epochs with the Adam optimizer and sparse categorical cross-entropy. On the held-out test set (n=93, balanced), the CNN classifier ran an accuracy of 92.5%, with an AUROC (Area Under the Receiver Operating Characteristic Curve) of 0.991 (Table 3) and a log loss of 0.144. Mars samples were predicted with high sensitivity (recall = 0.96), while Analog samples achieved higher precision (0.95), reflecting a relative feature balance across categories.

Table 1: Stage	1 Confusion	Matrix
	Analog(0)	Mars(1)
True $Analog(0)$	38	5
True Mars(1)	2	48

Table 2: Stage I Classification Report precision recall f1 support label Analog 0.9500000.8840000.91600043 Mars 0.9060000.9320000.96000050

(Table 2)

Table 3: Overall Stage I Metrics value 93 n_{eval} accuracy 0.924731auroc 0.991163 $average_precision$ NaN log_loss 0.143852 $pred_count_1$ 53 $pred_count_0$ 40 n_stage2 51 $pct_gated_to_stage2$ 54.838710

(Table 3)

A Gradient-weighted Class Activation Map (12) (Table 4) was created to analyze which regions the model perceived as the most common factors in classifying Mars images. Across multiple validation sets, model activations were concentrated mostly around geomorphic boundaries and stratigraphic layering, indicating that the model typically relied on such morphological traits, like those of channels and bedding planes to differentiate between terrain types.

Table 4	Sample I	Sample II (Image Not Included in the initial Dataset, extracted from MSL Curiosity Rover Raw Image Dataset) (14)
Original Image		
Grad-CAM output		

For the second stage of our analysis pipeline, outputs were further evaluated using a livability index L (scaled between 0 and 1). Among the 51 Mars-positive samples, the mean livability index was 0.417, with scores clustering at a midrange band of 0.31-0.48 (Table 5). These results suggest that most images were neutrally classified with the model neither stating high nor low livability rates across the tested data. Dust warnings were found to be common, with twenty-four samples flagged as "Warning", twenty-five as "Caution", and two as "Severe" (Table 6).

Table 5: Livability Index (L) Summary Statistics sd median p25p75 \min \mathbf{n} mean max \mathbf{L} 510.4169910.0407180.4268400.3886850.4454490.3129800.480751(Table 5)

Table 6: Dust Warning Levels		
	count	percent
bucket		
None	0	0.000000
Caution	25	49.019608
Warning	24	47.058824
Severe	2	3.921569
	(Table 6)	

Correlation analysis revealed that certain geomorphic proxies were strongly tied to livability index. The presence of layering, channel-like features, and ripples was the most significant positive aspect of livability. On the other hand, shelter and clast formations were negatively correlated, while dust obscured the majority of measurements.

Contributions were additionally observed from rock cover and fluvial complexity. These results suggest that stratification and channel morphology were the primary geomorphic indicators driving the livability index (Table 7), despite the weighted columns being geared towards a bigger emphasis on rock cover and fluvial evidence.

Table 7: Spearman Correlations with L $_{\rm rho}$ p_value \mathbf{n} proxy 0.762550has_layers 0.00000051has_channels_like 0.6525770.00000051has_ripples 0.5452060.00003551 has_shelters -0.473045 0.00045651rock_cover_moderate 0.3303170.01791751 fluvial_complexity 0.2483260.07890551dusty_cover_high 0.0857010.54986751

(Table 7)

DISCUSSION

The CNN scored a high classification accuracy of 92.5% when distinguishing between Curiosity snapshots from Earth analogs, along with an AUROC rate of 0.991. These scores indicate that the model can reliably differentiate unique geomorphic and photometric features in Martian terrains. The Grad-CAM visualizations reinforce this by showing that the network's attention was focused on boundaries, layering, and channel-like features. These features are widely regarded as strong indicators of habitability by planetary scientists (13).

Though the mean index score of 0.427 suggests that most images were neutral in their likelihood to support life, the found correlations (visually depicted through Table 5) reveal that stratified layering, channel morphology, and ripple patterns were the strongest positive contributors. These findings align relatively well with established astrobiological knowledge, since these features often point to historical water activity and other environments, which are known to support life (13). Negative correlations with clast distribution and sheltering suggest that certain terrain elements may either obscure signs of habitability or arise in conditions less likely to sustain life.

An interesting challenge within our model involved the implication of dust cover, where, in the weights, we kept the presence of dust in the analyzed images separate from the final proxy score. We ultimately adjusted our pilot-based weights due to the highly saturated number of flagged dust indicators, which often significantly lowered scores, as we had initially intended to consider such presence as a negative factor in our final livability score (Table 6). Our decision and findings to alter the final weights may indicate a complication in image clarity caused by the presence of dust, which commonly correlated with dramatic score reductions during our initial development cycle. Instead, dust functions seemed to appear more as a technical challenge for detection rather than a biological constraint.

These results emphasize computer vision's ability to distinguish between planetary surfaces and also to generally extract meaningful features for astrobiological inference. While current habitability assessments often rely on detecting chemical/geological analysis, our approach demonstrates that useful insights can be found from analyzing imaging data alone. These findings could greatly impact future missions where onboard computational tools may be able to offer more effective surface analysis, guiding sampling priorities, and reducing Earth-based manual annotation.

That said, several limitations should be noted. For one, the dataset size is quite small when compared to other computer vision applications, and relying on open source archives could introduce biases in the represented features. Additionally, the livability index is built on weights that were heuristically chosen. Refining these with scientific validation can improve the index's reliability. Though correlations between proxies and habitability scores were recognized, further testing with larger, more extensive datasets would be needed to fully substantiate these associations in order to merit usage in more hands-on environments.

CONCLUSION

This study presents a novel computer vision-based pipeline for estimating habitability likelihood from planetary surface imagery. By combining convolutional neural networks with geomorphic feature extraction, we demonstrated that planetary terrains can be analyzed for more than just binary classification, allowing for interpretable assessments that reflect the terrains' potential to be inhabited.

The findings show the real potential for integrating visual automated analysis into future missions. A livability index could help streamline time-consuming processes. It could help select landing/exploration sites and help find environments most favorable to life more quickly. Though preliminary, this work lays the base for a promising approach to astrobiological exploration that effectively utilizes visual datasets.

Future research should focus on refining the livability index with larger training sets and incorporating more surface proxies. Ultimately, the framework should be adjusted based on mission findings. With these developments, computer vision may very well become an essential tool in planetary science.

FUNDING SOURCES

This research did not receive any specific grant from funding agencies in the public, commercial, or non-profit sectors.

CONFLICT OF INTERESTS

The authors declare that there are no conflicts of interest related to this work.

REFERENCES

- 1. LU, Steven (ed.). Mars surface image (curiosity rover) labeled data set version 1 NASA open data portal. LU, Steven (ed.), NASA [online]. March 2025. [Accessed 5 October 2025]. Available from: https://data.nasa.gov/dataset/mars-surface-image-curiosity-rover-labeled-data-set-version-1
- 2. Yingst, R.A., M.E. Schmidt, and R.C.F. Lentz, Mars analog handlens-scale image database, EAR-E-REBELXT-7-IMAGE-MARS-ANALOG-V1.0, NASA Planetary Data System, 2009.
- 3. Bradski, G., The OpenCV Library. Dr. Dobb's Journal of Software Tools, 2000. Available from: https://opencv.org (accessed on 2025-10-05).

- 4. van der Walt, S., Schönberger, J. L., Nunez-Iglesias, J., Boulogne, F., Warner, J. D., Yager, N., Gouillart, E., Yu, T., and the scikit-image contributors. scikit-image: Image processing in Python. PeerJ, 2014, 2: e453. https://doi.org/10.7717/peerj.453
- 5. Abadi, M., Agarwal, A., Barham, P., Brevdo, E., Chen, Z., Citro, C., et al. TensorFlow: Large-scale machine learning on heterogeneous systems. 2015. Software available from: https://www.tensorflow.org (accessed on 2025-10-05).
- 6. Duda, R.O. and Hart, P.E., Use of the Hough transformation to detect lines and curves in pictures. Communications of the ACM, 1972. 15(1): 11–15.
- 7. Frangi, A.F., Niessen, W.J., Vincken, K.L., and Viergever, M.A., Multiscale vessel enhancement filtering. In: Wells, W.M., Colchester, A., and Delp, S. (eds), *Medical Image Computing and Computer-Assisted Intervention MICCAI'98*. Springer, Berlin, Heidelberg, 1998, Vol. 1496, pp. 130–137.
- 8. Zhang, T.Y. and Suen, C.Y., A fast parallel algorithm for thinning digital patterns. Communications of the ACM, 1984. 27(3): 236–239
- 9. Gabor, D. "Theory of Communication." Journal of the Institution of Electrical Engineers Part III: Radio and Communication Engineering, vol. 93, no. 26, 1946, pp. 429–457.
- 10. Shannon, C. E. "A Mathematical Theory of Communication." The Bell System Technical Journal, vol. 27, no. 3, 1948, pp. 379–423.
- 11. Sarkar, N., and Chaudhuri, B. B. An efficient differential box-counting approach to compute fractal dimension of image. IEEE Trans. Systems, Man, and Cybernetics, 1994, 24(1): 115–120.
- 12. Selvaraju, R. R., Cogswell, M., Das, A., *et al.* Grad-CAM: Visual explanations from deep networks via gradient-based localization. In: *ICCV* 2017, pp. 618–626
- 13. Carr, M. H. The Surface of Mars. Cambridge University Press, 2006. ISBN 978-0-521-87201-0.
- 14. NASA (ed.). Mars Science Laboratory (Curiosity) Raw Images. NASA, [online]. [no date]. [Accessed 5 October 2025]. Available from: https://mars.nasa.gov/msl/multimedia/raw-images/l
- 15. Williams, R.M.E., Irwin, R.P., Zimbelman, J.R., et al. Paleohydrologic analysis of branching ridges on Mars: Evidence for inverted fluvial channels. Journal of Geophysical Research: Planets, 2009, 114(E10). DOI: 10.1029/2009JE003349
- 16. Gonzalez, R.C. and Woods, R.E. Digital Image Processing. 4th ed., Pearson, 2018. ISBN 978-0-13-335672-4.
- 17. Kingma, D.P. and Ba, J. Adam: A Method for Stochastic Optimization. arXiv preprint, 2014, arXiv:1412.6980. Available from: https://arxiv.org/abs/1412.6980